286 Vol. 39, No. 1 / January 2022 / Journal of the Optical Society of America B Research Article

Journal of the Optical Society of America B OPTICAL PHYSICS

Ultrasensitive terahertz sensing in all-dielectric asymmetric metasurfaces based on quasi-BIC

Zhongfu Li,[1] Yuanjiang Xiang,[2] Shixiang Xu,[1] and Xiaoyu Dai[2,*]

[1]College of Physics and Optoelectronic Engineering, Shenzhen University, Shenzhen 518060, China
[2]School of Physics and Electronics, Hunan University, Changsha 410082, China
*Corresponding author: xiaoyudai@126.com

Received 7 September 2021; revised 21 October 2021; accepted 21 October 2021; posted 1 December 2021; published 17 December 2021

The bound state in the continuum (BIC), which supports exceptional resonance in the optical range, has attracted significant attention for its bright applications in sensors and other optical devices. However, it is difficult to cover the analyte's transmission/reflection spectrum since BIC possesses an infinite Q factor. In this work, we proposed a thoughtful all-dielectric columns structure with broken symmetry that supports quasi-BIC to achieve ultrasensitive sensing in the terahertz range. Our metasurfaces consist of a series of periodic unit cells, including two silicon columns with asymmetric cylindrical holes and a SiO_2 substrate. Quasi-BIC resonances can be observed by the transmission/reflection spectrum. The quasi-BIC resonances with a narrow frequency width are sensitive to the surrounding media and the sensitivity can achieve 170.58 GHz/RIU. We believe our ultrasensitive sensor with high performance and sensitivity provides an exciting platform for biosensing.

https://doi.org/10.1364/JOSAB.442660

1. INTRODUCTION

Sensing, one of the most important applications for terahertz (THz) technology, has attract much attention and been studied widely because of its high performance in nondestructive detection [1], label-free sensing [2], gas sensing, [3] biomedical imaging [4], and diagnosis and identification [5]. In particular, THz technology has great potential for applications in biosensing due to its strong penetration of biomaterials and its support for the special vibrational modes of the macromolecules of biomaterials such as DNA [6]. However, the poor sensitivity of THz technology has limited its further application in biosensing.

To break the poor sensitivity limit in the THz range, a perfect metamaterial absorber consisting of graphene and SiO_2 has been proposed [7,8]. Graphene surface plasmons (GSP) have a strong dependence on the adjacent dielectric, and the sensitivity can be improved using this GSP's property. But this perfect metamaterial absorber needs a thin layer graphene with a thickness of $t = 0.34\ nm$, which is difficult to achieve experimentally. Recently, all-dielectric metasurfaces with strong toroidal dipole (TD) resonance and a low Q factor have been proposed experimentally [9–11]. The structures proposed in these works are easy to manufacture; however, the low Q factor hinders their application in sensing. Some works reveal a link between the toroidal dipole resonance and the bound state in the continuum (BIC) [12,13]. Based on these works, terahertz sensing has been proposed with a high Q toroidal dipole resonance governed by bound states that have a $> 10^5$ Q factor. However, this work requires a manufacturing process with a precision of 0.4 μm, which is a great challenge for manufacturing asymmetric supersurfaces [14]. BIC, first proposed in quantum mechanics, is a general wave that can be observed in electromagnetic waves and acoustic waves. One of the most outstanding characteristics of BIC that exists only in lossless and perfect symmetry structures is an infinite Q factor plus an extremely narrow resonance [15,16]. Some works recently have been proposed to achieve BIC with different incidence angles [17,18].

Moreover, metasurfaces based on metal with a large local electromagnetic field enhancement and low Q factor have been put forward to enhance the interaction of THz waves and analytes. Although these system have achieved a sensitivity of >1 THz/RIU, the Q factors are limited to <10 because of inevitable nonradiative loss [19]. Therefore, it is important to find a resonance that is sensitive to the index of surrounding media and has a high Q factor. Recently, all-dielectric structures supporting BICs with an infinite Q factor have been proposed [20–22]. Its narrow resonance is sensitive to the index of surrounding media, which provides an ideal platform to design new ultrasensitive sensors.

In this work, an ultrasensitive sensor based on quasi-BIC resonance in the THz range is proposed. The unit cells of the structure consist of two columns with cylindrical holes and a substrate. The cylindrical holes arranged asymmetrically are used to excite quasi-BIC resonance with a high Q factor. Here, we consider only one polarization mode (the electric field is along the y direction and the incident angle of THz waves is 0°) and observe the transmission spectrum to study our sensor's performance.

This paper has four sections. First, the displacement current and electric field distribution at resonance frequency is studied. It reveals that the energy is local in two columns and the direction of displacement current depends on the location of the cylindrical holes. Next, we study the influence of the structure parameters, and it can be seen from the result that our system has quasi-BIC resonance. Then, by analyzing the shift of the narrow resonances when we change the index of the surrounding media, we can achieve a sensitivity of 170.58 GHz/RIU. Finally, we discuss the effect of the loss of Si on the transmission and Q factor.

2. STRUCTURE

The structure of our design breaks the symmetry and gets TD resonance. As mentioned in the introduction, the extremely narrow resonance with a high Q factor is necessary for the application of THz sensing. One of the easiest ways to get a high Q factor resonance is by exciting the BIC based on all-dielectric metamaterials. The BIC could be converted to quasi-BIC when we broke the symmetry in the plane perpendicular to the incident direction of THz wave [23]. A metallic metamaterial consisting of split-ring resonators was first proposed to achieve a transition between true BIC and the leaky resonance [24]. Then, many all-dielectric metamaterials with broken symmetry that support high Q factor Fano resonances [24–27] and TD resonances [12,28] were proposed.

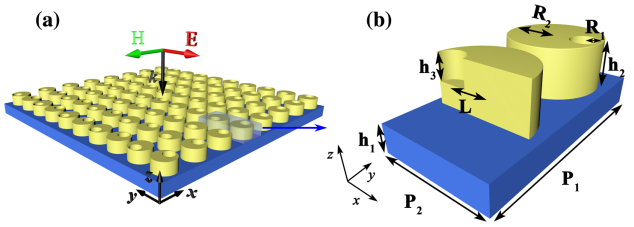

Fig. 1. Schematic of THz asymmetric all-dielectric metasurface structure. (a) Metasurface structure composing of $5*8$ unit cells. $\boldsymbol{E}$, $\boldsymbol{H}$, and $\boldsymbol{k}$ represent the polarization of the electric field, the magnetic field, and the incident direction. (b) Structure of one unit cell. The key parameters used in our calculations are: $P_1 = 200$ μm, $P_2 = 125$ μm, $h_1 = 45$ μm, $h_2 = 50$ μm, $h_3 = 0.5h_2$, $R_1 = 20$ μm, and $R_2 = 40$ μm.

In our designed metamaterials, the mirror symmetry, which can be represented as $(x, y) \rightarrow (x, -y)$ in the $x - y$ plane, was broken by the introduction of two cylinder holes. A schematic of the THz asymmetric all-dielectric metasurfaces sensor is illustrated in Fig. 1(a). Only $5*8$ unit cells are shown here, and the two adjacent columns along the x direction form one unit cell. Note that the location of cylinders is asymmetrical along the y direction and can be represented by asymmetric parameters L and $-L$, respectively, as shown in Fig. 1(b). This is one of the most important part of our design. Specifically, $L = 0$ means that the hole has no displacement in the x direction, and the two columns are symmetric in the $x - y$ plane. When the asymmetric parameter is $L \neq 0$, it means that the symmetry breaking is introduced in which the hole has a displacement of L in the opposite direction along the x direction. According to our study, the sign of L has no influence on the result, so we use the $+L$ in the following part of paper. Other parameters shown in Fig. 1(b) are set as $P_1 = 200$ μm, $P_2 = 125$ μm, $h_1 = 45$ μm, $h_2 = 50$ μm, $h_3 = 0.5h_2$, $R_1 = 20$ μm, and $R_2 = 40$ μm. The THz waves are incident from the $+z$ direction, where the electric field polarization is along the y direction. Then, we can get transmission/reflection spectrum from the spectrometer. Here, we only consider the transmission (T). The reflection (R) can be obtained by the following equation: $R = 1 - T$, where the absorption can be ignored. First of all, we show result of the transmission spectrum in Fig. 2(a). It can be seen that a resonance exists at 0.93 THz. To observe the localization of energy more clearly, the displacement current where the color and size of arrow represents its amplitude distribution on the surfaces and volume is plotted in Fig. 2(b). We can see that the

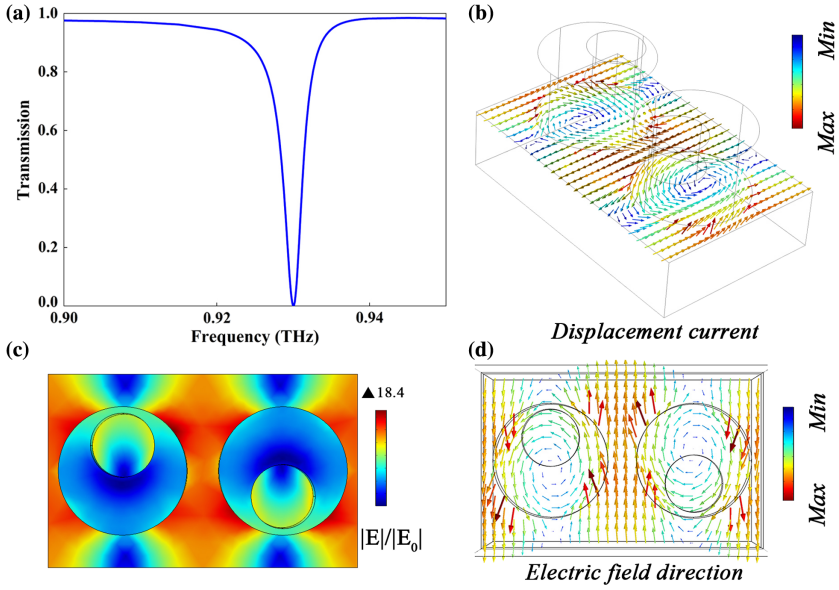

Fig. 2. (a) Transmission spectrum with different incident angles. (b) Displacement current distribution of substrate. Color represents the amplitude of the displacement current. (c) Electric field distribution in the surface of the unit cell.

energy in the two columns has opposite directions and forms a toroidal. Further, we calculated the electric field distribution and the electric field direction at resonance frequency, which are, respectively, shown in Figs. 2(c) and 2(d). We can see that most of the electric field is located near the bottom of the columns, which means that resonance is happening and two electric dipoles (ED) [29] exist within different columns.

3. RESULTS AND DISCUSSION

Next, we study the influence of symmetry (that is, the asymmetric parameter L) on the transmission spectrum, as shown in Fig. 3. From the simulation results, we can see that the quasi-BIC resonances convert to BICs, which have been marked by red dotted circles in Figs. 3(b) and 3(c) when the asymmetry parameter L equals to zero. This is caused because our designed structure supports true BIC when the symmetry is saved [30]. In fact, the true BIC is unstable against the broken symmetry, and the width of the narrow resonance increases as the symmetry is broken. From the simulation results in Fig. 3(a), we can see that the width of the resonance gradually increases as L increases and reaches the maximum width around $L = 0.5 * R_2$. This is because the area of the asymmetry of the two cylinders reaches a maximum near $L = 0.5$; in other words, our structure breaks the symmetry to the maximum extent at this time. However, the extremely narrow resonance has a high requirement on the observation device, and a large width of the resonance will reduce the sensitivity, so the asymmetry parameter $L = 0.4$ is chosen to continue the subsequent research. In Fig. 3(b), we show the transmission with a different L when the unit cell consists of only one column, while the results of Fig. 3(b) are obtained in the case of unit cells composed of two columns. By comparison, we can find that the resonance summit of the former is wider and more sensitive to asymmetric parameters. Similarly, a formant of quasi-BIC can be obtained because of the broken symmetry in the $x - y$ plane, which is reflected in the results as the breakpoint in Figs. 3(b) and 3(c).

Structural parameters such as the height and shape will affect the resonance properties when we design the metamaterials. The results of a numerical simulation show that when the radius R_2 (Fig. 1) of the cylinder is increased, the resonant frequency appears to blue shift with an increase in the resonance width, as shown in Fig. 4(d). At the same time, we can see in Fig. 4(a) that with the increase of substrate thickness h_1 (Fig. 1), the position of resonance appears to red shift with a decrease in the resonance width. Instead, the effect of the change in the height of the cylinder on the resonance is opposite to the change caused by the thickness of the base, which has been shown in Fig. 4(c). When we reduce the radius of the hole R_2 or increase the height h_2 of the columns, the volume of the remaining columns will become larger, which means that the ability to confine the electric field diminishes. The increase of the thickness h_1 of the cavity leads to an increase in the electrical length of the cavity in the z direction, resulting in a red shift of the resonance. Finally, to make it easy to detect the resonance and have a larger Q factor, we choose the parameters described in the Fig. 1 caption. For the selection of materials, we used the most common SiO_2 ($\varepsilon = 3.75$) and Si ($\varepsilon = 11.7$) as the substrate and columns cavity, respectively.

According to [31], the transmission of quasi-BIC can be described by the Fano formula, where the Fano parameters can be fit through the material and geometrical parameters of metasurface:

$$T(\omega) = \frac{T_0}{1+q^2}\frac{(q+x)^2}{1+x^2} + T_{\mathrm{bg}}(\omega), \tag{1}$$

where $x = 2(\omega - \omega_0)/\gamma$, γ and ω_0 are the inverse lifetime and resonant frequencies, and T_{bg} and T_0 are the background contribution of the nonresonant modes to the resonant peak amplitude and the offset, respectively. For quasi-BICs, the quality factor $Q = \omega_0/\gamma$ depends on α:

$$Q(\alpha) = Q_0[\alpha]^{-2}, \tag{2}$$

where α is the asymmetry parameter of our metasurface, and Q_0 is a constant that is 30 in our fitting result. In our structure, α is approximately equal to L. The Q factor as a function of the asymmetry parameter α is shown in Figs. 4(d) and 6(b). The infinite Q factor can be obtained at $\alpha = 0$, while the minimum Q factor can be obtained at $\alpha = 0.4$. According to the fitting line marked by the black line shown in Fig. 6, we can see that the Q factor and asymmetry α^{-2} are linear and the result is consistent with Eq. (2).

As we mentioned earlier, sharp resonances can be applied to extremely sensitive sensors for refractive index sensing. Therefore, we investigated our proposed sensitivity based on

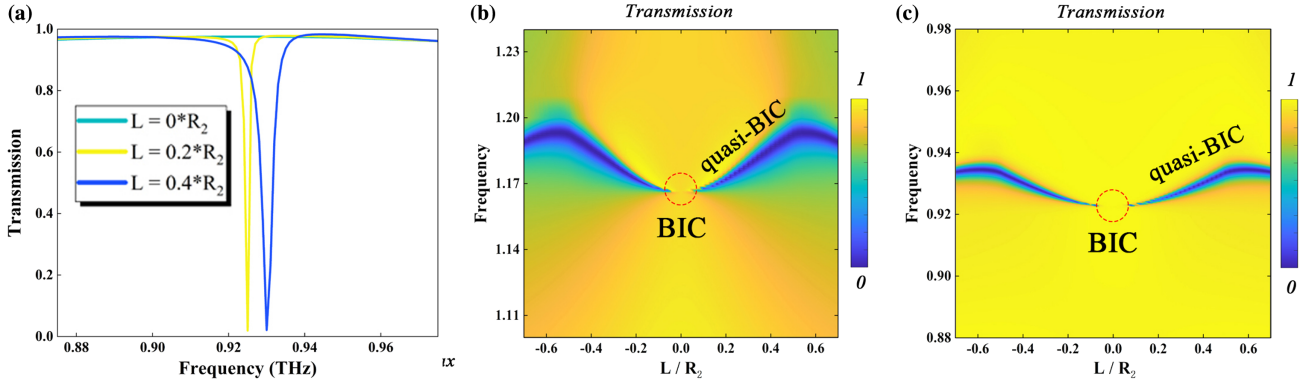

Fig. 3. Influence of asymmetric parameters L on resonances. (a) Transmission spectrum at cases of $L = 0 * R_2$, $L = 0.2 * R_2$, and $L = 0.4 * R_2$. (b) and (c) Transmission spectrum with different L. The red dotted circle marks the BIC. The results of (b) and (c) are the results obtained using the different structures shown in the inset.

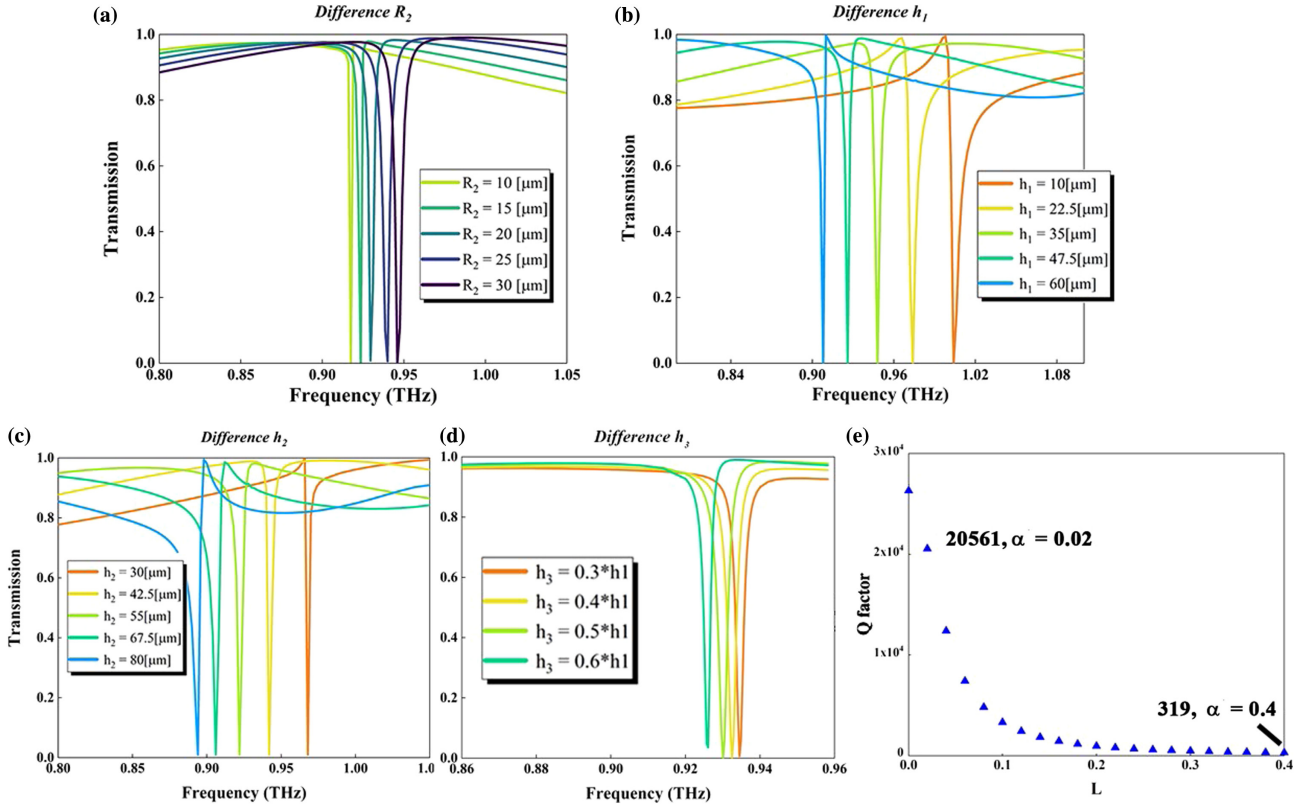

Fig. 4. Effect of structural parameters on resonance. (a) With an increase in R_2, the resonance appears to blue shift and the resonance width increases. (b) With an increase in h_1, the resonance appears to red shift and the resonance width decreases. (c) With an increase in h_2, the resonance appears to blue shift and the resonance width decreases. (d) With an increase in h_3, the resonance appears to blue shift and the resonance width decreases. (e) Q factor at difference L. The Q factor at $\alpha = 0.001$ and $\alpha = 0.4$ are 26313 and 319, respectively.

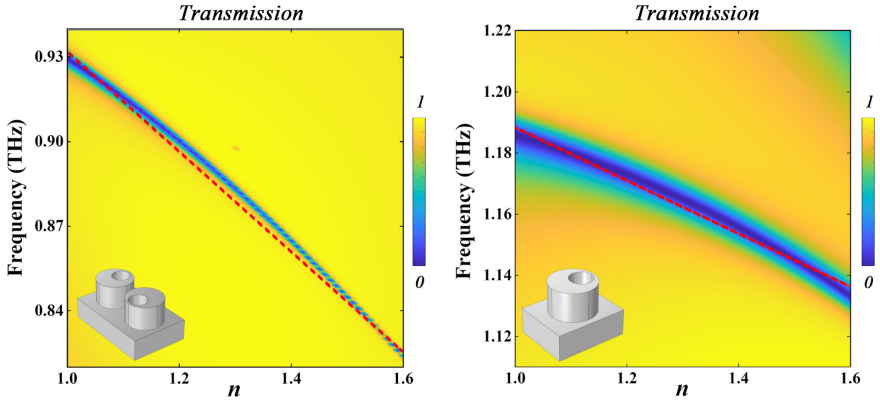

Fig. 5. (a) and (b) Changes in the transmission spectrum with different refractive indices under different structures. Color represents the amplitude of transmission. When $n = 1$, the resonance frequency in (a) and (b) are 0.93 THz and 1.185, respectively, while resonance frequency in (a) and (b) are 0.824 THz and 1.133 when $n = 1.6$.

asymmetric metasurface structures based on quasi-BIC by numerical simulations. According to our simulation results, when the refractive index of the surrounding environment changes from $n = 1$ to $n = 1.6$, the resonant frequency changes from 0.94 to 0.84 THz, as shown in Fig. 5(a). It also can be seen that the red shift of the resonance is basically linear with a change in the refractive index. This also shows that our ultrasensitive sensor can maintain a high level of sensitivity performance in a different analyte. In general, we use $S = \frac{df}{dn} = 170.58$ GHz/RIU to obtain the sensitivity of the resonance, where n represents the refractive index of the surrounding index. This is much more sensitive than previous work, which used 77 GHz/RIU [32], 105 GHz/RIU [33], and 139.2 GHz/RIU [34]. For contrast, we study the sensitivity performance of the second structure, which has been plotted in the inset of Fig. 5(b). It can be seen from the results that the resonance also has a blue shift that is linearly associated with the refractive index, but the resonance width is wider compared

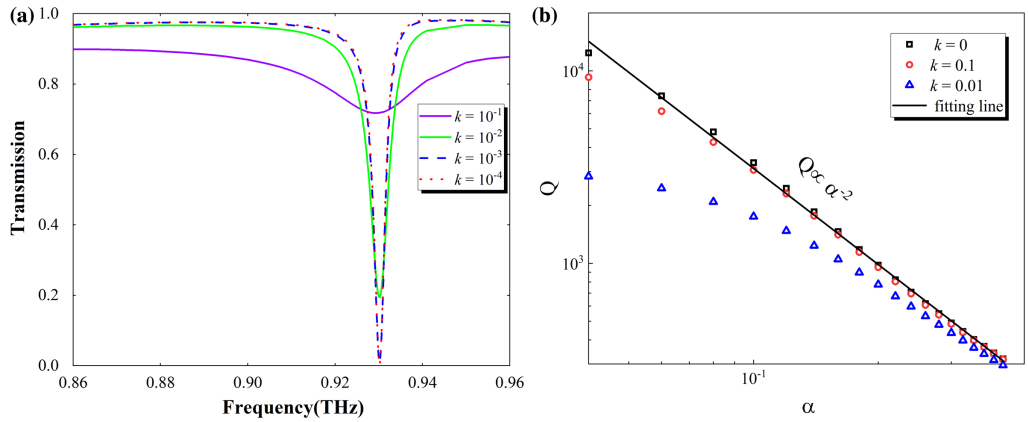

Fig. 6. Effect of loss coefficient on the result of transmission and Q factor. (a) Purple, green, blue, and red lines represent the loss coefficients $k = 10^{-1}$, 10^{-2}, 10^{-3} and 10^{-4}, respectively. (b) Black square, red circle, and blue triangle represent the Q factor with loss coefficients $k = 10^{-1}$, 10^{-2}, and 10^{-3}. The black line is the fitting curve.

to Fig. 5(a). Similarly, we can calculate that the sensitivity is 83.7 GHz/RIU, which is almost one-third of the first structure. From the analysis of the above results, we have realized the ultrasensitive sensor numerically by breaking the symmetry of the $x - y$ plane.

Finally, we discuss the effect of the loss coefficient and finite size on the calculation result. First, we calculate the transmission spectrum with a different loss coefficient of Si, which can been found in Fig. 6(a). Purple, green, blue, and red lines represent the loss coefficients $k = 10^{-1}$, 10^{-2}, 10^{-3}, and 10^{-4} respectively. The results show that loss coefficient of Si has no effect on the location of the resonance mode. Therefore, the sensitivity is unaffected by the loss coefficient. However, the Q factor shown in Fig. 6 is greatly affected by the loss coefficient of Si. In addition, the Q factor is greatly influenced by the finite size and the Q factor assessment of the finite size can be found in [35].

4. CONCLUSION

In conclusion, we propose and theoretically analyze a terahertz sensor with a high Q in all dielectric metasurfaces based on quasi-BIC, achieving a sensitivity of up to 170.58 GHz/RIU. The unit cell of structure of the metasurface consists of two columns with a cylinder hole. The quasi-BIC was obtained by breaking the symmetry in the $x - y$ plane by adjusting the position of the cylinder holes, which can be clearly seen in the simulation results. Further, we simulated and analyzed the electric field and energy distribution at the resonance frequency under different incident angles. The effects of different structural parameters on the formant and Q factor were also simulated and analyzed, and the conversion from quasi-BIC to Fano resonance was realized. Finally, we analyzed the performance of the sensor we designed, and the final numerical simulation results can reach a sensitivity of 170.58 GHz/RIU.

Funding. Natural Science Foundation of Hunan Province (2021JJ30135, 2021JJ30149); Science and Technology Planning Project of Shenzhen Municipality (JCYJ20180508152903208, JCYJ20190808143801672, JCYJ20190808150803580); National Natural Science Foundation of China (11874269, 61875133, 92050203)

Disclosures. The authors declare no conflicts of interest.

Data Availability. Data underlying the results presented in this paper are not publicly available at this time but may be obtained from the authors upon reasonable request.

REFERENCES

1. I. Amenabar, F. Lopez, and A. Mendikute, "In introductory review to THz non-destructive testing of composite mater," J. Infrared Millim. Terahertz Waves **34**, 152–169 (2013).
2. M. Nagel, P. Haring Bolivar, M. Brucherseifer, H. Kurz, A. Bosserhoff, and R. Büttner, "Integrated THz technology for label-free genetic diagnostics," Appl. Phys. Lett. **80**, 154–156 (2002).
3. D. M. Mittleman, R. H. Jacobsen, R. Neelamani, R. G. Baraniuk, and M. C. Nuss, "Gas sensing using terahertz time-domain spectroscopy," Appl. Phys. B **67**, 379–390 (1998).
4. S. M. Kim, F. Hatami, J. S. Harris, A. W. Kurian, J. Ford, D. King, G. Scalari, M. Giovannini, N. Hoyler, J. Faist, and G. Harris, "Biomedical terahertz imaging with a quantum cascade laser," Appl. Phys. Lett. **88**, 153903 (2006).
5. J.-H. Son, *Terahertz Biomedical Science and Technology* (CRC Press, 2014).
6. T. Globus, D. Woolard, T. Khromova, T. Crowe, M. Bykhovskaia, B. Gelmont, J. Hesler, and A. Samuels, "THz-spectroscopy of biological molecules," J. Biol. Phys. **29**, 89–100 (2003).
7. M. Nagel, F. Richter, P. Haring-Bolivar, and H. Kurz, "A functionalized THz sensor for marker-free DNA analysis," Phys. Med. Biol. **48**, 3625 (2003).
8. M. Nejat and N. Nozhat, "Ultrasensitive THz refractive index sensor based on a controllable perfect MTM absorber," IEEE Sens. J. **19**, 10490–10497 (2019).
9. D. C. Zografopoulos, A. Ferraro, J. F. Algorri, P. Martín-Mateos, B. García-Cámara, A. Moreno-Oyervides, V. Krozer, P. Acedo, R. Vergaz, J. M. Sánchez-Pena, and R. Beccherelli, "All-dielectric silicon metasurface with strong subterahertz toroidal dipole resonance," Adv. Opt. Mater. **7**, 1900777 (2019).
10. D. C. Zografopoulos, J. F. Algorri, W. Fuscaldo, J. M. López-Higuera, R. Vergaz, J. M. Sánchez-Pena, I.-A. Karolos, R. Beccherelli, V. E. Tsioukas, T. V. Yioultsis, and E. E. Kriezis, "All-dielectric toroidal metasurfaces for angular-dependent resonant polarization beam splitting," Adv. Opt. Mater. **9**, 2002143 (2021).
11. D. C. Zografopoulos, J. F. Algorri, A. Ferraro, B. García-Cámara, J. M. Sánchez-Pena, and R. Beccherelli, "Toroidal metasurface resonances in microwave waveguides," Sci. Rep. **9**, 7544 (2019).
12. Y. He, G. Guo, T. Feng, Y. Xu, and A. E. Miroshnichenko, "Toroidal dipole bound states in the continuum," Phys. Rev. B **98**, 161112 (2018).

13. X. Chen, W. Fan, and H. Yan, "Toroidal dipole bound states in the continuum metasurfaces for terahertz nanofilm sensing," Opt. Express **28**, 17102–17112 (2020).
14. Y. Wang, Z. Han, Y. Du, and J. Qin, "Ultrasensitive terahertz sensing with high-q toroidal dipole resonance governed by bound states in the continuum in all-dielectric metasurface," Nanophotonics **10**, 1295–1307 (2021).
15. A. F. Sadreev, "Interference traps waves in an open system: bound states in the continuum," Rep. Prog. Phys. **84**, 055901 (2021).
16. C. W. Hsu, B. Zhen, A. D. Stone, J. D. Joannopoulos, and M. Soljačić, "Bound states in the continuum," Nat. Rev. Mater. **1**, 16048 (2016).
17. J. Algorri, F. Dell'Olio, P. Roldán-Varona, L. Rodríguez-Cobo, J. López-Higuera, J. Sánchez-Pena, and D. Zografopoulos, "Strongly resonant silicon slot metasurfaces with symmetry-protected bound states in the continuum," Opt. Express **29**, 10374–10385 (2021).
18. S. Xie, S. Xie, G. Tian, Z. Li, J. Zhan, Q. Liu, and C. Xie, "Bound states in the continuum of nanohole array with symmetry broken in THz," Optik **225**, 165761 (2021).
19. Y. Yang, I. I. Kravchenko, D. P. Briggs, and J. Valentine, "All-dielectric metasurface analogue of electromagnetically induced transparency," Nat. Commun. **5**, 5753 (2014).
20. S. Li, C. Zhou, T. Liu, and S. Xiao, "Symmetry-protected bound states in the continuum supported by all-dielectric metasurfaces," Phys. Rev. A **100**, 063803 (2019).
21. F. Wu, J. Wu, Z. Guo, H. Jiang, Y. Sun, Y. Li, J. Ren, and H. Chen, "Giant enhancement of the Goos-Hänchen shift assisted by quasibound states in the continuum," Phys. Rev. Appl. **12**, 014028 (2019).
22. F. Wu, M. Luo, J. Wu, C. Fan, X. Qi, Y. Jian, D. Liu, S. Xiao, G. Chen, H. Jiang, Y. Sun, and H. Chen, "Dual quasibound states in the continuum in compound grating waveguide structures for large positive and negative Goos-Hänchen shifts with perfect reflection," Phys. Rev. A **104**, 023518 (2021).
23. D. Liu, F. Wu, R. Yang, L. Chen, X. He, and F. Liu, "Quasi-bound states in the continuum in metal complementary periodic cross-shaped resonators at terahertz frequencies," Opt. Lett. **46**, 4370–4373 (2021).
24. V. V. Khardikov, E. O. Iarko, and S. L. Prosvirnin, "Trapping of light by metal arrays," J. Opt. **12**, 045102 (2010).
25. K. Koshelev, Y. Tang, K. Li, D.-Y. Choi, G. Li, and Y. Kivshar, "Nonlinear metasurfaces governed by bound states in the continuum," ACS Photon. **6**, 1639–1644 (2019).
26. A. E. Miroshnichenko and Y. S. Kivshar, "Fano resonances in all-dielectric oligomers," Nano Lett. **12**, 6459–6463 (2012).
27. K. E. Chong, B. Hopkins, I. Staude, A. E. Miroshnichenko, J. Dominguez, M. Decker, D. N. Neshev, I. Brener, and Y. S. Kivshar, "Observation of Fano resonances in all-dielectric nanoparticle oligomers," Small **10**, 1985–1990 (2014).
28. H. M. Doeleman, F. Monticone, W. den Hollander, A. Alù, and A. F. Koenderink, "Experimental observation of a polarization vortex at an optical bound state in the continuum," Nat. Photonics **12**, 397–401 (2018).
29. Q. Zhao, J. Zhou, F. Zhang, and D. Lippens, "Mie resonance-based dielectric metamaterials," Mater. Today **12**(12), 60–69 (2009).
30. K. Koshelev, G. Favraud, A. Bogdanov, Y. Kivshar, and A. Fratalocchi, "Nonradiating photonics with resonant dielectric nanostructures," Nanophotonics **8**, 725–745 (2019).
31. K. Koshelev, S. Lepeshov, M. Liu, A. Bogdanov, and Y. Kivshar, "Asymmetric metasurfaces with high-q resonances governed by bound states in the continuum," Phys. Rev. Lett. **121**, 193903 (2018).
32. Y. Zhong, L. Du, Q. Liu, L. Zhu, K. Meng, Y. Zou, and B. Zhang, "Ultrasensitive specific sensor based on all-dielectric metasurfaces in the terahertz range," RSC Adv. **10**, 33018–33025 (2020).
33. Q. Xie, G.-X. Dong, B.-X. Wang, and W.-Q. Huang, "High-Q Fano resonance in terahertz frequency based on an asymmetric metamaterial resonator," Nano. Res. Lett. **13**, 294 (2018).
34. R. Yahiaoui, S. Tan, L. Cong, R. Singh, F. Yan, and W. Zhang, "Multispectral terahertz sensing with highly flexible ultrathin metamaterial absorber," J. Appl. Phys. **118**, 083103 (2015).
35. L. K. Warne, R. E. Jorgenson, and S. Campione, "Quality factor assessment of finite-size all-dielectric metasurfaces at the magnetic dipole resonance," Nanomater. Nanotechnol. **8**, 184798041882016 (2018).